RESEARCH METHODS

Anticipating the occurrence and type of critical transitions

Florian Grziwotz[1]†, Chun-Wei Chang[2,3]†, Vasilis Dakos[4], Egbert H. van Nes[5], Markus Schwarzländer[6], Oliver Kamps[7], Martin Heßler[7,8], Isao T. Tokuda[9], Arndt Telschow[1,10]*, Chih-hao Hsieh[3,11,12,13]*

Critical transition can occur in many real-world systems. The ability to forecast the occurrence of transition is of major interest in a range of contexts. Various early warning signals (EWSs) have been developed to anticipate the coming critical transition or distinguish types of transition. However, no effective method allows to establish practical threshold indicating the condition when the critical transition is most likely to occur. Here, we introduce a powerful EWS, named dynamical eigenvalue (DEV), that is rooted in bifurcation theory of dynamical systems to estimate the dominant eigenvalue of the system. Theoretically, the absolute value of DEV approaches 1 when the system approaches bifurcation, while its position in the complex plane indicates the type of transition. We demonstrate the efficacy of the DEV approach in model systems with known bifurcation types and also test the DEV approach on various critical transitions in real-world systems.

INTRODUCTION

There is a growing consensus that many real-world systems have a critical threshold (i.e., tipping point) (*1*, *2*), at which systems suddenly shift to a distinct state, i.e., critical transitions initiated by local bifurcation (*3*), for example, the outbreak of desert locust (*4*), development of psychiatric disorders (*5*), or rapid global warming at the end of glacial periods (*6*). Critical transitions may shift a system to a new state with undesirable properties, causing damage and loss in environmental, economic, and public health resources if corrective action is not taken in a timely manner. Thus, it is important for various fields of science and in many applications to forecast occurrence and consequence of critical transitions.

Under these circumstances, many early warning signals (EWSs) have been proposed to anticipate upcoming critical transitions (*7*). However, most EWSs can only warn of a critical transition in a qualitative way or do not perform consistently for different types of critical transition. According to bifurcation theory, when the system is approaching a tipping point, the system starts to recover more slowly from local perturbations (*8*–*10*), as the dominant eigenvalue goes to 0 in continuous systems or to 1 in discrete systems. This is called critical slowing down (*7*), and it can be revealed by the increase of generic EWS (*8*), such as increasing autocorrelation [e.g., AR1 (*2*)] and variability [e.g., SD (*11*)] in time series. Previous studies (*2*, *7*) suggest that AR1 and SD will reach 1 and infinity, respectively, at the tipping point, provided that the dynamical systems can be locally approximated by a first-order stochastic process. However, these thresholds were usually not met in real-world critical transitions (*2*) or even in model systems (*12*, *13*). For example, AR1 does not reach 1 for Neimark-Sacker bifurcation (fig. S1). The existing EWSs are developed for anticipating the critical transitions in fold bifurcation (*14*) [i.e., catastrophe shift (*1*)], but it is still difficult to distinguish fold bifurcation from more complex types of bifurcations (*14*, *15*) (e.g., Hopf or Neimark-Sacker bifurcation).

With understanding that different types of bifurcation bring divergent consequences to our focal systems that need different corresponding management to minimize potential losses, a recent study using deep-learning approach shows skill to distinguish types of bifurcation (*15*); however, this approach cannot tell the upcoming critical transition and is not rooted in the theory of dynamical system. Moreover, the method based on deep-learning strongly depends on the training set and is so far difficult to be applied in high-dimensional cases. Practically, there is no method providing a precise threshold for indicating how large the raised EWS shall be, beyond which critical transition is deemed to occur, and simultaneously indicating the type of transition.

The solution for the challenge is hinted in bifurcation theory—the types and conditions for the occurrence of critical transition are quantitatively determined on the basis of the dominant eigenvalue derived from locally linearized dynamical systems around an equilibrium (e.g., fixpoint or limit cycle) (*3*, *16*) (i.e., Jacobian matrices; Fig. 1). When the critical transition occurs at the tipping point, the absolute value of the dominant eigenvalue increases to 1 (in discrete systems) (*17*). Moreover, different bifurcation types are distinguishable by examining the dominant eigenvalue on complex plane (*17*). While these theoretical arguments are well established, a critical challenge in their implementation remains that such dominant eigenvalue can only be derived if numerical values of the equilibrium and all parametric equations governing dynamical systems can be

[1]Institute for Evolution and Biodiversity, Westphalian Wilhelms-University Münster, Münster 48149, Germany. [2]Institute of Fisheries Science, Department of Life Science, National Taiwan University, Taipei 10617, Taiwan. [3]National Center for Theoretical Sciences, Taipei 10617, Taiwan. [4]ISEM, CNRS, University of Montpellier, IRD, EPHE, Montpellier, France. [5]Department of Environmental Science, Wageningen University, Wageningen P.O. Box 47, 6700 AA, Netherlands. [6]Institute of Plant Biology and Biotechnology, University of Münster, Münster 48143, Germany. [7]Center for Nonlinear Science, Westphalian Wilhelms-University Münster, Münster 48149, Germany. [8]Institute for Theoretical Physics, Westphalian Wilhelms-University Münster, Münster 48149, Germany. [9]Department of Mechanical Engineering, Ritsumeikan University, Kusatsu 525-8577, Japan. [10]Institute for Environmental Systems Science, University of Osnabrück, Osnabrück 49076, Germany. [11]Institute of Oceanography, National Taiwan University, Taipei 10617, Taiwan. [12]Institute of Ecology and Evolutionary Biology, Department of Life Science, National Taiwan University, Taipei 10617, Taiwan. [13]Research Center for Environmental Changes, Academia Sinica, Taipei 11529, Taiwan.
*Corresponding author. Email: telschow@uni-muenster.de (A.T.); chsieh@ntu.edu.tw (C.-h.H.)
†These authors contributed equally to this work.

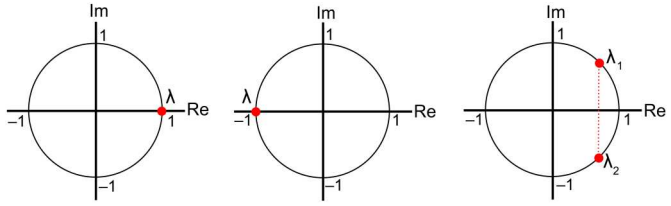

Bifurcation	Change in invariant sets	Dominant eigen-value λ
Fold	Appearance or disappearance of stable and unstable equilibria	$Im(\lambda)=0$ and $Re(\lambda) \rightarrow 1$
Period-doubling	Doubling the periods of limit cycles	$Im(\lambda)=0$ and $Re(\lambda) \rightarrow -1$
Neimark-Sacker	Appearance of a closed invariant curve	$Im(\lambda_{1/2}) \neq 0$ and $\lvert\lambda_{1/2}\rvert \rightarrow 1$

Fig. 1. Schematic illustration of the dominant eigenvalue in complex plane at the bifurcation point for different types of bifurcation. Mathematically, bifurcation can be recognized by changes in the dominant eigenvalue, λ, of the Jacobian matrix, **J**, at the equilibrium. See the "Information about bifurcations" section in Materials and Methods for more detailed explanation.

determined. However, equilibrium values are often difficult to estimate and the equations (or the parameters of the equations) are generally unknown (or difficult to estimate) in real-world systems.

Recent advances in time series analysis of dynamical systems indicate that Jacobian (interaction) matrix as well as its dominant eigenvalue can be estimated by the recently advanced lag-embedding empirical dynamical modeling (EDM) (*18*, *19*). This approach requires neither knowledge of the underlying equations nor numerical estimates of the equilibrium since the local Jacobians of the current state of the system are directly estimated from time series. However, the existing method of computing dominant eigenvalue (known as local Lyapunov stability) (*18*) requires full information of all interacting components (e.g., time series data of interacting species) that is usually not readily available, especially in large systems. Therefore, the existing method used to quantify dominant eigenvalue (*18*) might not be a suitable EWS and cannot be easily applied in majority of systems.

We propose dynamical eigenvalue (DEV) as a novel EWS derived from EDM that analyzes time series data requiring no specific model assumption (*20*) [e.g., no need to assume time-varying autocorrelated stochastic process (*21*)]. As above, local Jacobians are estimated by state space reconstruction (SSR) and without calculating equilibrium values. The proposed DEV thus directly estimates the dominant eigenvalue of focal systems instead of indirectly quantifying those phenomena accompanying with critical slowing down as previous EWS. Therefore, as suggested in bifurcation theory, this novel EWS has a quantitative threshold for the occurrence of critical transition (the absolute value of the estimated dominant eigenvalue $|DEV| = 1$) and enables to differentiate types of critical transition by examining DEV on complex plane (Fig. 1 presents the critical transitions induced by fold, period-doubling, and Neimark-Sacker bifurcations). The presence of DEV threshold enables us to not only present a qualitative increasing/decreasing trend of EWS in a relative sense (like most existing EWS) but also explicitly quantify system resilience in an absolute sense. That is, the absolute value of DEV itself is meaningful and can be directly compared to a theoretical threshold rather than just compared to values estimated in previous time windows. Unlike the existing EDM method in computing dominant eigenvalue (*18*), DEV recovers the whole system dynamics from a single time series using lag embeddings [i.e., Takens embedding theorem (*22*)], requiring no full information of interacting components. Implementation of DEV also relaxes the assumption underlying general EDM methods (*18*, *19*) that critical properties of the system (e.g., model parameters) are constant throughout the sampling period. This assumption unlikely holds in critical transition, during which at least one bifurcation parameter changes with time (*12*). Therefore, the proposed DEV enables to track temporal changes in system resilience (see details in Materials and Methods) and is rooted in bifurcation theory that quantitatively reveals both the occurrence condition and type of critical transition (*17*).

To validate the efficacy of DEV approach, we used three model time series datasets demonstrating known fold, period-doubling, and Neimark-Sacker bifurcations. Then, we empirically tested the DEV method in real-world cases of critical transitions from cell-level experiments to global-scale paleoclimatic events (tables S1 and S2). For each dataset, we computed DEV that anticipated the occurrence and type of critical transition in both model and empirical cases, following procedures summarized in fig. S2.

RESULTS

Validation of DEV using model data

We examined three discrete-time nonlinear dynamical models (table S1), Noy-Meir model, Hénon map, and Rosenzweig-MacArthur model (Fig. 2, A and B), representing the fold, period-doubling, and Neimark-Sacker bifurcation, respectively. Our analyses indicated that the derived DEV reliably estimated the dominant eigenvalues of nonlinear dynamical systems and mimicked its dynamical behavior when approaching bifurcation. Specifically, |DEV| monotonically increased when approaching the tipping point and reached 1 when the system was at the tipping point (Fig. 2C). Moreover, mapping DEV to the complex plane distinguished various types of bifurcations (Fig. 2D), where $Re(DEV) \rightarrow 1$ and $Im(DEV) \rightarrow 0$ for fold bifurcation, $Re(DEV) \rightarrow -1$ and $Im(DEV) \rightarrow 0$ for period-doubling bifurcation, and $Im(DEV) \neq 0$ and $|DEV| \rightarrow 1$ for Neimark-Sacker bifurcation. Consequently, the estimated DEV as a reliable EWS anticipated the occurrence of critical transition (i.e., tipping point) (Fig. 2C) regardless of bifurcation type. Results obtained from discrete-time models were similar to that obtained from their continuous-time analogs (fig. S3). These analyses indicated that DEV was an effective EWS that anticipated the occurrence of critical transition with a certain threshold ($|DEV| = 1$) and correctly distinguished various types of bifurcation in model systems. Being able to distinguish types of bifurcation is critical; for example, catastrophic shift (fold bifurcation) and increasing fluctuation (period-doubling bifurcation leading to chaos) cause different consequences in systems and require different ways of responses.

Next, we evaluated efficacy of the method when including noise (e.g., observation error and process noise). In the presence of noise, DEV remains a proper EWS (figs. S4 to S6) that monotonically increases when approaching the tipping points, but the quantitative threshold of |DEV| was not necessarily equal to 1 at the tipping

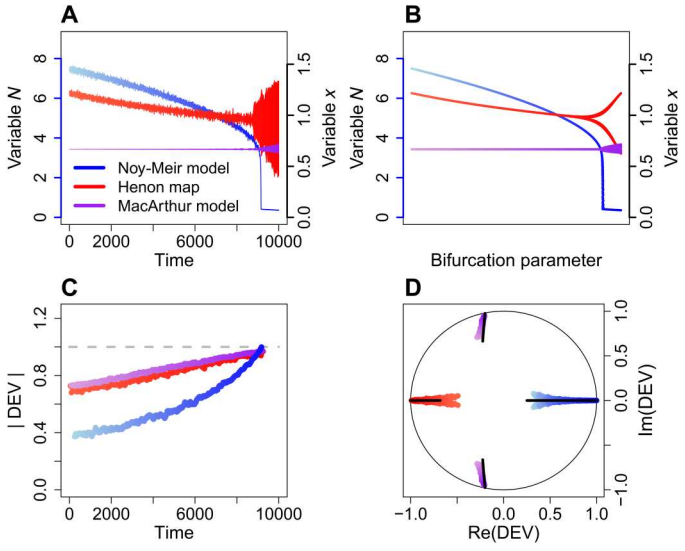

Fig. 2. Efficacy of DEV method as EWS indicating critical transitions in the three mathematical models. (**A**) Exemplary time series of the Noy-Meir model (blue), Hénon map (red), and Rosenzweig-MacArthur model (purple). (**B**) The bifurcation diagram illustrates effects of changing bifurcation parameters (see table S1 for parameter values) on the averaged variable states calculated from moving windows. (**C**) Estimated |DEV| increase over time and approach 1 at the bifurcation point [shown in (A) and (B)]. (**D**) Classification of bifurcation types based on |DEV| estimates on the complex plane (sensu Fig. 1). The |DEV| estimates move from interior of the unit circle toward the border through time, signaling critical transition; the color gradients from light to dark present time progression from initial time to the time right before critical transitions. Note that for each eigenvalue with a nonzero imaginary part, a pair of conjugated eigenvalues exists and shows mirror symmetry on the complex plane. In (D), the minor values in the imaginary axis appear in the Noy-Meir model (blue) and Hénon map (red), owing to process noises included in the models. Black lines within the circle labeled the theoretical dominant eigenvalues.

point. Nevertheless, under small to moderate levels of noises, DEV still correctly identified types of bifurcation (fig. S7). On the basis of this sensitivity analysis, the estimated DEV in model systems remained effective under noises, except for the Rosenzweig-MacArthur model, which was more sensitive to observation noise (fig. S6). Perhaps the Rosenzweig-MacArthur model showing Neimark-Sacker bifurcation has more complicated mathematical normal form (*23*) with higher-order terms likely amplifying impacts of noises. Nonetheless, under reasonable degree of noises, our DEV method remains effective in revealing Neimark-Sacker bifurcation that occurred in real-world cases (e.g., Fig. 3, D to F).

DEV analysis of empirical time series

We investigated five empirical examples, including a cyanobacteria microcosm experiment under light stress, a physical experiment of voice production during phonation onset, cytosolic adenosine triphosphate (ATP) dynamics in living plant tissues under progressive hypoxia, calcium carbonate ($CaCO_3$) abundance by the end of greenhouse Earth, and bus voltage frequency before power grid failure (tables S1 and S2) and anticipated the occurrence and type of critical transition (Fig. 3). For empirical systems, |DEV| increased when approaching to the tipping point and almost reached 1 at the tipping point (Fig. 3, B, E, H, K, and N). Therefore, we inferred that the theoretical threshold (|DEV| = 1) was still meaningful in empirical systems, despite noises in empirical data. In addition, the computed DEV differentiated the types of critical transition in empirical cases (Fig. 3, C, F, I, L, and O). Among these examples, only the voice experiment had Neimark-Sacker bifurcation (with nonzero imaginary part), whereas all others demonstrated fold bifurcation. Furthermore, this conclusion was robust against various choices of embedding parameters (e.g., E, τ, and window size) (figs. S8 to S12). Identification of bifurcation type provided important insight into foreseeing the coming new state of the system. Fold-type critical transition shifts systems to a new regime with a distinct state (e.g., Fig. 3J), whereas a Neimark-Sacker bifurcation shifted the system to a new regime exhibiting higher temporal variability (e.g., Fig. 3D). Therefore, with information regarding bifurcation type, more appropriate management strategies can be prepared to cope with new regimes.

Reliability tests of DEV method

Although DEV is a quantitative EWS with theoretical threshold, its efficacy is likely undermined by observation and process noises (e.g., |DEV| < 1 and more gradual increase of |DEV| when approaching bifurcation; figs. S4 to S6). Underestimation of DEV under strong noises was likely due to the dominant eigenvalue of pure stochastic processes being 0, which leads the synthesized signals with the DEV less than 1 at the tipping point. Hence, a precautionary approach is needed when considering the derived DEV, especially at the tipping point. Here, we suggest that the uncertainty of DEV can be evaluated by its predictability on future states [e.g., the correlation coefficient (ρ) between observed and predicted one-step forward future states; Fig. 4] because predictability is an effective indicator to evaluating the uncertainty of reconstructed dynamical systems (*24*). There was a high association between the predictability and the uncertainty of estimated DEV defined as how far the estimated DEV was to the analytically solved dominant eigenvalue (when without noise). When predictability was high, |DEV| reached almost 1 before transition; in comparison, |DEV| did not reach 1 (figs. S4 to S6) when the predictability was low under strong noises (Fig. 4). Thus, system predictability gives an indication for a precautionary decision of the threshold.

DISCUSSION

Implications from analyzing empirical data

On the basis of analyses of empirical data, the DEV method can be applied to various fields of science (Fig. 3). This is remarkable because of not only diverse underlying systems but also the huge differences with respect to the temporal and spatial scales that range from milliseconds and micrometers in cellular processes to millions of years and thousands of kilometers in climate dynamics. Nonetheless, there was consistently one common feature: Underlying dynamics are governed by feedback mechanisms, a typical characteristic of nonlinear dynamical systems. Such feedback regulations might lose controls due to external forcing; consequently, a critical transition occurs (*16*). Therefore, an analytical framework that acknowledges feedbacks and nonlinearity, e.g., our DEV method rooted in nonlinear time series analysis (*25*), has wide applicability for anticipating occurrence of critical transition under various spatiotemporal scales.

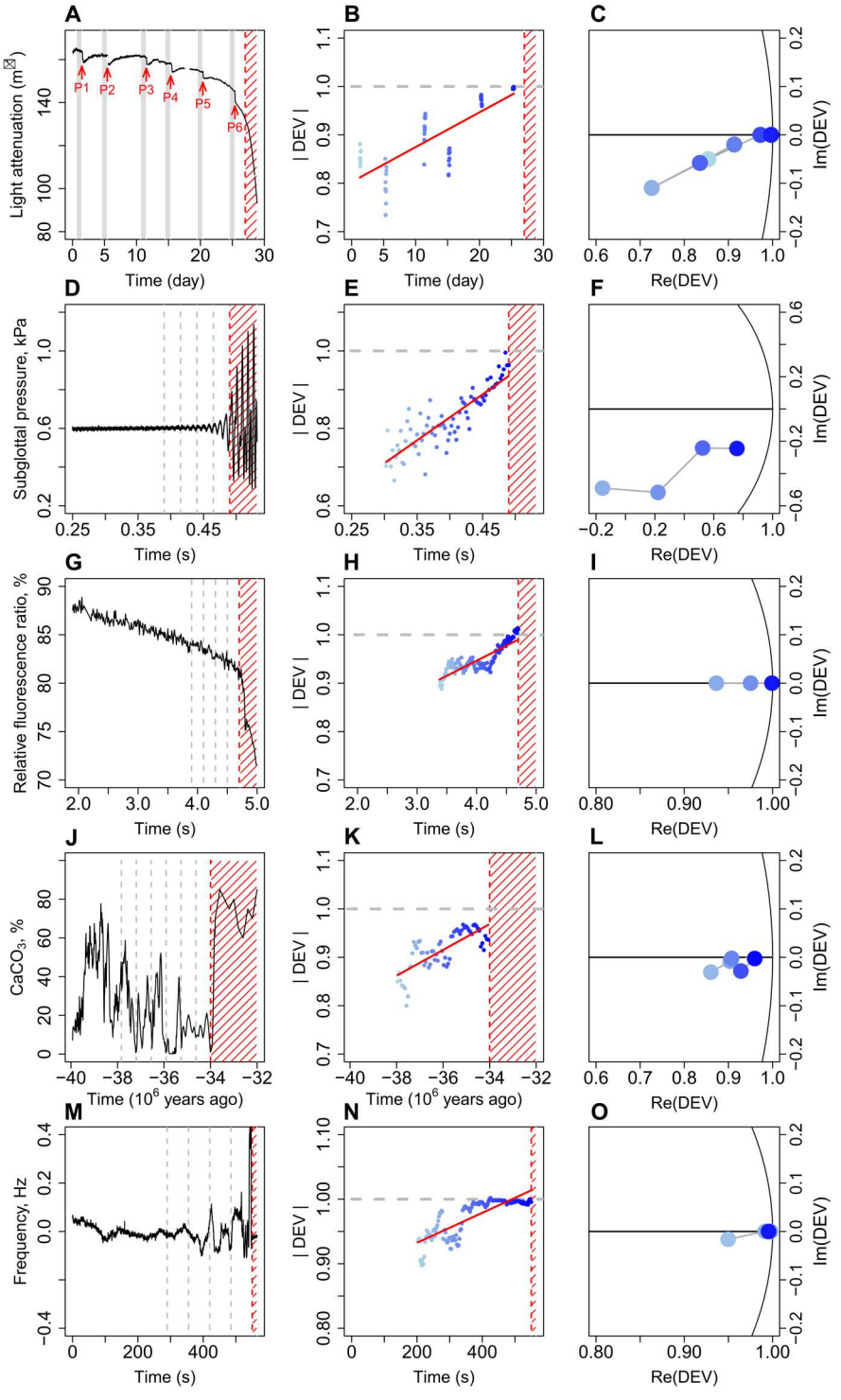

Fig. 3. Empirical evaluations showing that |DEV|s can be EWS for critical transition and indicate type of bifurcation. |DEV|s signal: fold bifurcation in a microcosm experiment of a cyanobacteria population undergoing dilution perturbations and increasing light stress (**A** to **C**), Neimark-Sacker bifurcation in an experiment of voice onset under increasing flow rate (measured subglottal pressure) (**D** to **F**), fold bifurcation in an in vivo biosensing experiment of cytosolic ATP at progressing hypoxia (**G** to **I**), fold bifurcation in climate data of $CaCO_3$ abundance in sediments from the end of the last greenhouse Earth (**J** to **L**), and fold bifurcation in electricity data of "1996 Western North America blackouts" (**M** to **O**). (A), (D), (G), (J), and (M) illustrate time series data; the red dashed area delineates the regime after critical transition. In (A), arrows indicate external perturbations, and we estimated |DEV|s from the 250 data points (~1 day) before each perturbation (gray area). (B), (E), (H), (K), and (N) illustrate the time series of estimated |DEV|; the red lines derived from the linear regression of |DEV| versus time, and the |DEV| value of 1 (gray dash line) indicates the bifurcation point. (C), (F), (I), (L), and (O) indicate type of bifurcation. For better visualization, in (C), we averaged |DEV| estimates associated with the same perturbations event; in (F), (I), (L), and (O), |DEV| estimates are averaged in time intervals before the bifurcation [delineated by dashed lines in (D), (G), (J), and (M)]. The color gradients from light to dark present time progression from initial time to the time right before critical transitions.

Existing methods for anticipating a critical transition are qualitative in the sense that statements can be made only about whether or not a system is moving toward a tipping point. In comparison, the most novel aspect of the DEV method is that a quantitative statement can be made about how far the current DEV values from the theoretical threshold (i.e., |DEV| = 1) that presents a more rigorously defined bifurcation (*17*) (i.e., critical transition). In addition to being an EWS, this quantitative feature makes assessing system resilience possible even if the analysis was only done within one time window including a few portions of time series data. For example, the |DEV| values estimated from the last time windows before critical transition (300 data points) are equal to 0.99, 0.99, 1.01, 0.91, and 0.99 for the microcosm data, the voice data, the cellular energy data, the climate data, and the power grid data, respectively,

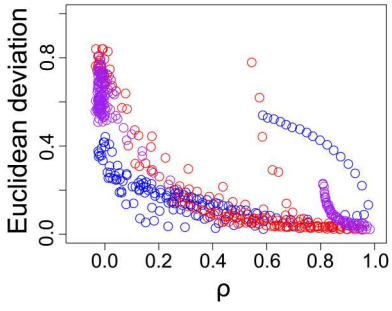

Fig. 4. Uncertainty of DEV as a function of predictability (ρ) for the mathematical models with different combinations of noises. The results of the Noy-Meir model (blue), Hénon map (red), and Rosenzweig-MacArthur model (purple) under a specific combination of observation noise and process error are shown. Each curve was obtained by plotting the uncertainty (defined as the Euclidean distance between the analytic eigenvalue and the estimated DEV in complex plane) as a function of predictability (ρ) measured within each moving window in the DEV analysis. For all combinations of noises, the uncertainty decreased by increasing the one-step forward predictability. In addition, there is no noticeable difference between the analytically solved and DEV derived eigenvalue when the predictability was high (e.g., $\rho > 0.8$). Thus, the one-step forward predictability can be used to evaluate the reliability of DEV as quantitative EWS.

indicating that all examined system states were either approaching or just at a tipping point. In other words, the DEV measures correctly anticipated the ongoing critical transition without relying on measures estimated in previous time windows (i.e., a need to uncover a trend of declining system resilience in a relative sense). Although great care must be taken with estimates, the DEV method is a major step forward in improving the accuracy of the resilience and risk assessment of a wide variety of empirical systems.

DEV analysis of the microcosm experiment presents a novel way to quantitatively forecast catastrophic consequences of biological populations. A central issue in population biology is to predict fates of populations (e.g., sustained or extinction of species or species invasion) when facing various stressors. Although predictions can be made from numerous models, implementation of most population models requires correct identification of both model structure and parameters (*26*), which is seldomly possible in empirical cases. In contrast, our DEV analysis characterized population dynamics in the absence of detailed information about model structure and parameter. Nonetheless, unlike most model-free EWS (*27*), DEV as an empirical estimate of dominant eigenvalue allows them to be analyzed as in theoretical population models (e.g., bifurcation analysis). Therefore, the proposed DEV links model-free EWS to the analysis of parametric models and offers a novel and promising research direction.

Exceptionally good results were achieved for cellular energy status and voice production (Fig. 3, D to I). This may hint toward cell biology and physiology as promising areas for future DEV applications. Both research fields have been rarely mentioned in previous EWS literature, although many types of time series data with high spatiotemporal resolution can be generated using modern imaging and omics techniques. Therefore, DEV may have broad applications, including investigating various cellular and physiological switches that are critical to organism functions. These switches often lead to diseases (e.g., cancers), whereas dysfunction in energy transformation within mitochondria has well-established links to aging (*28*) or disease (*29*). Along this research line, our proposed DEV may serve as a warning signal in the early stages of disease development, as treatment timing is often crucial for treatment responses.

Critical transition has important roles in driving climate events at global scales (Fig. 3, J to L). Our findings confirmed the previous report (*2*) that a critical transition occurred by the end of the last greenhouse Earth phase. Our proposed method further characterized this global-scale shift as a case of fold bifurcation. In this case, mean air temperature underwent abrupt declines and then terminated greenhouse Earth. Compared to the analyses of other empirical cases (Fig. 3, B, E, H, and N), the DEV measures derived from paleoclimate data, though substantially increased, had noticeable underestimation around the tipping point (i.e., <1 in Fig. 3K). Such underestimation may have been caused by the noises introduced when inferring ancient climate conditions from geological climate proxy or by lacking spatial information (i.e., time series from a single site) in analyzing global-scale climate dynamics that is inherently spatial.

Our analysis of voltage frequency data right before a power grid failure (Fig. 3, M to O) suggested a critical transition of electric systems. Maintaining a stable power grid requires sophisticated regulation to balance supply and demand of electricity, considering the complex interactions between meteorological and socioeconomic factors and the various sources of energy. Considering urgent needs in electricity management, particularly in changing environments, our DEV analysis provided an opportunity for monitoring the resilience of power grids at millisecond scales. For example, a real-time grid resilience based on our quantitative warning signal could help network operators to prevent power grid failures when the whole grid is moving toward a tipping point.

Efficacy of DEV as EWS

Our proposed DEV is a proper EWS, showing consistent early warning patterns (e.g., monotonic increase trend) when approaching the tipping point, in both models and empirical datasets (Figs. 2 and 3). Compared to previously proposed generic EWS, such as autocorrelation (e.g., AR1) and variability (e.g., SD), autocorrelation and variability had reliable early warning patterns in fold and period-doubling bifurcation (fig. S1) as suggested in previous studies (*7*, *30*); however, they did not perform well in Neimark-Sacker bifurcation wherein the increasing trend of AR1 was minor and did not reach 1 and the increasing trend of variability was less marked (fig. S1). When applying AR1 and variability indices on empirical cases (fig. S13), early warning patterns were not always observed (e.g., fig. S13, B, H, and I). Perhaps this reflected distinct sensitivity of the generic EWS to various types of bifurcation. In addition, some EWSs relying on variability (e.g., SD) are likely more sensitive to process noises (e.g., figs. S4E and S5E).

It is worthy to discuss the theoretical connection between DEV and AR1. Mathematically, if a dynamical system can be approximated by a first-order linear stochastic process (i.e., AR1 process) for the chosen time window, the matrix **J** (Eq. 1 in Materials and Method) governing the evolution of dynamical system can be formularized as a simple diagonal matrix (i.e., $\mathbf{J}_{AR1}$) with all diagonal elements equal to the estimated AR1. Here, $\mathbf{J}_{AR1}$ was assumed fixed within the analyzed time window, in contrast to the matrix **J** estimated in DEV that can vary within a time window. Obviously, the dominant eigenvalue of this matrix $\mathbf{J}_{AR1}$ is equal to AR1.

Therefore, according to bifurcation theory, AR1 theoretically reaches 1 at the tipping point in fold bifurcation, as suggested (*2*, *7*). However, convergence of AR1 to 1 requires that the dynamical system can be well approximated by first-order stochastic process for the chosen time window. Following the same mathematical reasoning, AR1 approaches to −1 for period-doubling bifurcation because the dominant eigenvalue will reach −1 around the tipping point; this was confirmed by our analysis of Hénon map (fig. S1). However, in any case, the approximation of AR1 process can only obtain the real-valued dominant eigenvalue because the estimated AR1 can never be a complex number. This explains why AR1 cannot be applied to Neimark-Sacker or other types of bifurcations in which the imaginary parts of dominant eigenvalues are always preserved. This mathematical reasoning also suggests that only fold bifurcation can exhibit high similarity between the current and previous system states (X_t and X_{t+1}) (*2*) (i.e., increasing AR1) before critical transition. However, this phenomenon might not necessarily occur in the other types of bifurcation that manifested only minor increases (e.g., Neimark-Sacker bifurcation in Rosenzweig-MacArthur model) or even decreased (e.g., period-doubling bifurcation) in AR1 (fig. S1). Therefore, from the bifurcation theory viewpoint, application of AR1 for detecting critical transition is a special case of DEV.

Limitations of DEV and forward looking

To evaluate the efficacy of DEV approach on more complex models, we first investigated a stochasticity-driven, patch dynamics model that exhibited no early earning signal (quantified as variance) before critical transition (see details in text S1 and fig. S14A) (*31*). For such a system with explicit spatial information, we examined whether our DEV approach was still effective. In our study, DEV derived from embedding time series of multiple patches (i.e., multivariate DEV; fig. S14, B and C) had a distinct EWS near the tipping point, but the DEV derived from embedding time series of a single patch (i.e., univariate DEV; fig. S14D) did not work. This confirmed previous analysis (*32*), suggesting that explicit spatial information is necessary to detect the EWS of the critical transition originating from strong spatial processes (*32*). In that sense, multivariate DEV can be complimentary to other EWS relying on spatial patterns (*33*, *34*). Multivariate DEV can be applied not only in a dynamical system with explicit spatial information but also in systems consisting of more than one variable, such as a Hénon map (fig. S15). Along this research line, we noted that several new EWSs based on multivariate time series data perform better than do classic EWSs (AR1 and variance), for example, multiple spatial times series (*35*) or multiple species time series (*36*). Therefore, a more general DEV framework combing both univariate and multivariate DEV paves a new research direction that may help detect critical transition emerging from diverse mechanisms, such as spatial processes or multispecies interactions. Regardless, more detailed investigations are needed for developing EWS in more complex systems.

Then, we explored the influences of system dimensionality on the efficacy of DEV, based on analysis of dynamical models with higher dimensions. Specifically, we investigated multispecies Ricker models composed of various numbers of species (see details in text S2 and fig. S16). Model analyses suggested that the efficacy of DEV in anticipating the upcoming period-doubling bifurcation was not equally good among all interacting components (i.e., various species in the model), although the increments of |DEV| were mostly positive (fig. S16, E to H). Such divergences can be more readily apparent in systems with higher dimensionality, wherein more |DEV|s did not reach 1 before the tipping. Declines in DEV efficacy when increasing system dimensionality were probably caused by the localization phenomenon in interaction networks (*37*, *38*), meaning that influences of bifurcation that occurred in some network nodes may not necessarily propagate across the entire networks but be localized within a group of nodes. In that regard, some network nodes with certain topological features (*38*) can be less sensitive to dynamical changes compared to other network nodes, especially in a weakly coupled interaction network, e.g., multispecies Ricker model. Nonetheless, identifying species that enable to demonstrate clear bifurcation patterns remains a challenging task (*39*) and thus warrants more detailed investigations from a network perspective. Although we investigated only the period-doubling bifurcation using multispecies Ricker models, the difficulty when dealing with high-dimensional systems likely also occurs in fold and Neimark-Sacker bifurcation. In addition to the issue of spatial processes and the issue of high dimensionality, we also addressed the limitations of DEV for ill-posed cases in text S3.

The embedding approach has been used to evaluate system stability; these studies estimated the dominant eigenvalues based on the single time window (i.e., using the whole time series) (*18*, *40*). Here, we show that, as the standard procedure used for EWS estimations, the moving window approach used to compute DEV (fig. S2) was necessary. Further analyses indicated that the dominant eigenvalue derived from the single time window approach (fig. S17) cannot reveal reliable early warning patterns and failed to identify the period-doubling bifurcation (fig. S17F). These results confirmed that a moving window approach is necessary for computation of EWS, as some important properties [e.g., nonlinearity (*41*)] of dynamical systems changed when the system approached a tipping point.

Interpretation of DEV findings requires knowledge of differences between classical bifurcation theory and the model-free EDM framework used in our DEV analysis. Although the DEV method is motivated in large part by mathematical bifurcation theory, implementation of DEV method based on a model-free EDM analysis is very different from classic bifurcation analysis. In classical bifurcation theory, stability of a dynamical system (usually around equilibria) is determined by the standard analysis of Jacobian matrices (Fig. 1) that can be derived only when the governing equations (e.g., a system of coupled differential equations) are known. In contrast, the model-free framework of EDM used in DEV facilitates access to the stability of dynamical system via the estimated dominant eigenvalue without explicitly identifying the governing equation or equilibria. In addition, compared to the classical bifurcation analysis around equilibria, EDM-based approaches can be more generally applied in real-world systems with complicated dynamics because the local Lyapunov stability derived in DEV can even be evaluated in chaotic systems (*42*) in which nontrivial equilibria may not exist.

Our DEV approach performed reasonably well in models and empirical data; however, its underlying mathematical evaluation has not been fully established. Although local Lyapunov stability derived from time-delayed embedding is theoretically invariant to that from the original system (*42*), the DEV approach, strictly speaking, cannot simply borrow the mathematics of classic bifurcation theory, for the following reasons. First, the DEV approach is

based on EDM with model-free features (*20*); although model-free features provide flexibility to investigate more general dynamical systems, such features hinder deeply rooting DEV in specific mathematical proofs. Second, although DEV can be used to anticipate the bifurcations under a certain degree of noise (figs. S4 to S7), the transient dynamics induced by noises may change system states suddenly and discontinuously. Because those new states can be so different from its original trajectory, it might cause a transient increase in a nondominant eigenvalue or make the dominant eigenvalues temporarily >1 (i.e., "unstable" DEV values), although the system has not gone through a critical transition. In other words, an unstable eigenvalue does not necessarily indicate a critical transition; rather, it could just be a consequence of rapid movement toward a distant equilibrium. Consequently, the classic interpretation of eigenvalues with respect to bifurcation points no longer holds, and our decision about whether those states are close to the bifurcation or not can be qualitatively changed. Regardless, the problems of transient dynamics are, to some extent, alleviated in our DEV method as revealed in our analyses (figs. S4 to S7) because the dominant eigenvalues estimated at each time point were averaged over a certain interval within the time window. Furthermore, if a system consistently stayed near the critical boundary (i.e., falling near the margin of the unit circle) due to slowly changing bifurcation parameters, then it is almost certainly being pushed either toward an equilibrium (or limit cycle). In such cases, the dominant eigenvalue will shrink or be drawn toward a critical transition when exceeding the critical threshold. These complexities create a challenging task to provide detailed mathematical evaluation for application of DEV in anticipating bifurcations and thus require further investigations.

In conclusion, the DEV approach developed in this study proposes an empirical EWS with the quantitative threshold to anticipate the occurrence of critical transition and simultaneously identify type of bifurcation. Although the efficacy of DEV is likely undermined by measurement and process noises, DEV has great potential to effectively anticipate the occurrence and type of critical transition with a more precautionary defined threshold. Because both occurrence condition and bifurcation type can be unambiguously revealed, this approach potentially brings great values to real-world management, making timely and effective responses when facing new regimes.

MATERIALS AND METHODS

Information about bifurcations

Critical transition is initiated from local bifurcation, which results from destabilization of equilibria of dynamical system accompanied with appearance and disappearance of invariant sets (Fig. 1) (*43*). Mathematically, bifurcation can be recognized by changes in the dominant eigenvalue, λ, of the Jacobian matrix, **J**, at the equilibrium. The Jacobian matrix **J** of an *n*-dimensional dynamical system is defined as

$$\mathbf{J} = \begin{pmatrix} \frac{\partial f_1}{\partial x_1} & \frac{\partial f_1}{\partial x_2} & \cdots & \frac{\partial f_1}{\partial x_n} \\ \frac{\partial f_2}{\partial x_1} & \frac{\partial f_2}{\partial x_2} & \cdots & \frac{\partial f_2}{\partial x_n} \\ \vdots & \ddots & \ddots & \vdots \\ \frac{\partial f_n}{\partial x_1} & \frac{\partial f_n}{\partial x_2} & \cdots & \frac{\partial f_n}{\partial x_n} \end{pmatrix}$$

where *n* functions $f_1(x_1,..., x_n),..., f_n(x_1,..., x_n)$ describe the dynamics of *n* variables $x_1,..., x_n$, respectively. On the basis of the dominant eigenvalues of Jacobian matrices at equilibrium, three types of bifurcation, including the fold (or saddle-node), the period-doubling (or flip), and the Neimark-Sacker (or Hopf) bifurcations (*43*), can be explicitly distinguished in complex plane (Fig. 1).

However, recent studies indicated that the dominant eigenvalue at each time point can be inferred from local Jacobian matrices at the current state of the system based on time series by reconstructing the local linear approximations of the dynamics in state space (see the "EWS based on the dominant eigenvalue" section). Such estimated time-dependent dominant eigenvalue has been used to infer local Lyapunov stability. Because time series data are discrete, the absolute value of the dominant eigenvalue reaches 1 (i.e., $|\lambda| \rightarrow 1$) at the bifurcation point in all types of bifurcations. Note that the time series data simulated from continuous systems, such as differential equations, are also discrete as they are solved numerically. The properties of dominant eigenvalues inferring the bifurcations in continuous systems are described in fig. S3.

Empirical dynamic modeling

Our DEV approach is rooted in the framework of EDM. According to the theory of dynamical systems, a system can be described as a set of states (e.g., attractor), whose evolution over time is determined by a set of rules (e.g., equations). These rules describe how the state of attractor changes as a function of interacting variables. Motion on the attractor can be projected onto the coordinate axis of associated variables, forming time series; conversely, time series of the interacting variables can be projected back to the multidimensional state space to recover the attractor (*44*). Therefore, knowing the state and the set of rules that govern the underlying system is equivalent to knowing the time series of all interacting variables. When studying empirical systems, the set of rules is unknown. Meanwhile, very likely, only one or few variables are measured, and their interactions are unknown a priori. However, it is possible to reconstruct a topologically invariant shadow version of the attractor using time delayed scalar measurements of a single dynamical variable: $X_t = (x_t, x_{t-\tau}, ..., x_{t-(E-1)\tau})'$, where x_i are observations at time point *i*, *E* is the embedding dimension, and τ is the time lag. This idea, called SSR, is based on Sauer *et al.*'s extension (*45*) of Takens' theorem (*22*) for dynamical systems. An illustration of the SSR concept is apparent in the following animation: tinyurl.com/EDM-intro. Because of topological invariance, the reconstructed attractor preserves the essential mathematical features of the original dynamical system. SSR enables investigation of dynamic properties of the system, such as interactions [e.g. Jacobian (*25*)] and stability (*18*, *19*), as well as transitions between stable and unstable states (*41*).

EWS based on the dominant eigenvalue

Among properties of dynamical systems, a critical issue of practical importance is being able to identify and predict critical transition. Mathematically, critical transitions are associated with local bifurcations, i.e., qualitative changes in system behavior due to changes in parameter. Bifurcations result from appearance and disappearance of invariant sets due to changes in stability (*46*) and can be recognized by changed eigenvalues of the Jacobian matrix derived from local linear approximation around a fixed point (i.e., local Jacobian) (*9*).

Critical transitions can be classified according to changes in the dominant eigenvalue, λ, of local Jacobian. In general, three types of critical transitions/bifurcations can be defined: the fold (tangent), the period-doubling (flip), and the Neimark-Sacker (Hopf) bifurcations (*43*). If a discrete system undergoes a fold bifurcation, stable and unstable equilibriums collide and annihilate, or an equilibrium appears suddenly. Fold bifurcation is indicated by the dominant eigenvalue reaching Re(λ) = 1 and |λ| = 1. For period-doubling bifurcation, a regularly repeating series of points double in its period when the bifurcation occurs. Consecutive period-doublings lead to chaos in dynamical systems. The period-doubling bifurcation is indicated by the dominant eigenvalue reaching Re(λ) = −1 and |λ| = 1. If a system undergoes a Neimark-Sacker bifurcation, a closed invariant curve appears from an equilibrium. This is indicated by a pair of conjugated dominant eigenvalues with $\mathrm{Im}(\lambda_{1/2}) \neq 0$ reaching $|\lambda_{1/2}| = 1$.

A methodological challenge is then how to estimate local Jacobian in each time point so as to track its change through time. In state space, the Jacobian is the local linear approximation of the dynamical system. To reconstruct the Jacobian at point X_N, Eckmann and Ruelle (*47*) proposed an idea that minimizes the squared error, $\mathrm{error}^2 = \frac{1}{\#\mathcal{U}} \sum_{X_i \in \mathcal{U}} \|X_{i+1} - \mathbf{J}X_i - \nu\|^2$, with respect to the coefficients of matrix **J** and some offset vector ν, given the set $\mathcal{U}$ of all neighbors of X_N with a distance smaller than a defined value, ϵ. 03F5;. This basic idea has been adapted in a previous algorithm (*48*) to calculate local Jacobians and to estimate Lyapunov exponents from observed time series. However, a critical issue of these algorithms is to determine the size of $\mathcal{U}$. If $\mathcal{U}$ is too small, the system is underrepresented, the coefficients of matrix **J** cannot be reliably estimated, and the algorithms are sensitive to noises. In contrast, if $\mathcal{U}$ is too big, noise becomes less important, but one might lose track of the underlying nonlinear dynamics (*46*).

In this study, we estimated the local Jacobian using an S-map (*19*, *25*), which has been shown to overcome problems associated with selecting $\mathcal{U}$ and to account for system nonlinearity. In detail, S-map involves generating an E-dimensional embedding (univariate or multivariate). The state space at time t is given by $X_t = [x_t, x_{t-\tau}, \ldots, x_{t-(E-1)\tau}]^T$. For each target time point t_a, the S-map algorithm computes a local linear model $\boldsymbol{C}$ that predicts the future value $Y_{t_a+\tau}$ using the vector X_{t_a} from the reconstructed state space. That is

$$Y_{t_a+\tau} = C_0 + \sum_{j=1}^{E} C_j \, x_{t_a-(j-1)\tau}$$

The linear model is fitted to the other vectors in the state space. However, in contrast to linear regression models, linear approximation in S-map is done only locally by giving greater weighting to the points that are close to the target point, X_{t_a}. The model $\boldsymbol{C}$ is the singular value decomposition solution to the equation

$$B = \boldsymbol{A} \cdot C$$

where B is an n-dimensional vector (n is the number of observations) of the weighted future values of Y_{t_i} for each historical point, t_i, given by

$$B_i = w(\|X_{t_i} - X_t\|^2) Y_{t_i+\tau}$$

and $\boldsymbol{A}$ is then $n \times E$ dimensional matrix given by

$$A_{ij} = w(\|X_{t_i} - X_t\|^2) x_{t_i-(j-1)\tau}$$

The weighting function w is defined by

$$w(d) = \exp\left(-\frac{\theta d}{\overline{d}}\right)$$

where $\|\cdot\|^2$ denotes the Euclidean distance and $\overline{d}$ is the average distance between Y_{t^*} and all other vectors on the attractor. The extent of this weighting is tuned by the nonlinear parameter $\theta \geq 0$. Note that the model C is separately calculated for each time point, t^*. Thus, C potentially differs for each time point of the time series. As recently shown, the coefficients of the local linear model provided by C are an approximation of local Jacobians (*18*, *25*) that can be used as a proxy of the interaction strength between embedded variables.

The original algorithm proposed in Deyle *et al.* (*25*) aimed to estimate local Jacobians of the current state of the system using multivariate time series of interacting variables. However, the same algorithms can be used for embedded time series from a single variable following the concept of lagged coordinate embedding (i.e., univariate embedding). Here, we aimed to estimate the coefficients of $X_{t+\tau} = \mathbf{J}X_t + \nu$ with respect to matrix **J** and offset vector ν. Since the reconstructed state space is a delay embedding space of a univariate time series, almost all elements of the Jacobian, **J**, are zero, except the lower-off diagonal, which are unity, and except the first row, which contains the nontrivial linear approximation. The same argument holds for the offset vector ν. Here, the linearized dynamics read

$$\begin{pmatrix} x_{t+\tau} \\ x_t \\ \vdots \\ x_{t-(E-2)\tau} \end{pmatrix} = \begin{pmatrix} j_{11} & \cdots & \cdots & j_{1E} \\ 1 & 0 & \ldots & 0 \\ & \ddots & \ddots & \vdots \\ 0 & & & \\ \ldots & 0 & 1 & 0 \end{pmatrix} \begin{pmatrix} x_t \\ \vdots \\ x_{t-(E-2)\tau} \\ x_{t-(E-1)\tau} \end{pmatrix} + \begin{pmatrix} \nu_1 \\ 0 \\ \vdots \\ 0 \end{pmatrix} \quad (1)$$

Following the S-map algorithm, matrix **J** of parameters $j_{11}, \ldots, j_{1E}$ can be calculated as the associated S-map coefficients (*18*, *25*). Because **J** is evaluated at each time point [i.e., local Jacobian **J**(t)], it is time varying. With the Jacobians, we can calculate the dominant eigenvalue for each local Jacobian through time and evaluate the system's local Lyapunov stability (as an EWS of critical transition), and we can further identify the type of critical transition (Fig. 1). As the dominant eigenvalue changes through time, we name this indicator DEV. DEV allows us to anticipate occurrence and type of critical transition (fig. S2).

Our approach focused on local estimates of the Jacobian matrix around the actual state of the system, rather than around a putative equilibrium point implied by the local Jacobian matrix [e.g., following a similar concept proposed by Cenci and Saavedra (*19*)]. The mathematics behind the classic bifurcation theory are rooted at the analysis at equilibrium conditions, whereas our DEV approach evaluated the local Lyapunov stability. Thus, strictly speaking, the

DEV approach cannot simply borrow the mathematics of classic bifurcation theory; thus, further mathematical study is warranted.

Model data

To demonstrate the efficacy of the DEV approach, we analyzed three representative models with distinct types of critical transition, including Noy-Meir model (fold bifurcation), Hénon map (period-doubling bifurcation), and a discrete version of the Rosenzweig-MacArthur model (Neimark-Sacker bifurcation). In these model simulations, bifurcation parameters are chosen to demonstrate critical transitions. Equations of the three models are demonstrated below.

The Noy-Meir model (*49*) is described by the following equations

$$N_{t+1} = N_t \exp(0.75 - 0.1N_t) - F\frac{N_t^2}{N_t^2 + 0.75^2} + \omega_t \zeta N_t \quad (2)$$

The bifurcation parameter F was linearly increased from 0 to 2 throughout the whole simulated time series.

The Hénon map (*50*) reads as

$$x_{t+1} = 1 - ax_t^2 + y_t + \omega_t \zeta x_t \quad (3)$$

$$y_{t+1} = 0.3x_t \quad (4)$$

The bifurcation parameter a was linearly increased from 0.1 to 0.4 throughout the whole simulated time series.

Last, the Rosenzweig-MacArthur model (*51*) reads as

$$x_{t+1} = (1 + l)x_t - 4{x_t}^2 - \frac{x_t y_t}{1 + 0.5x_t} + \omega_t \zeta x_t \quad (5)$$

$$y_{t+1} = -2y_t + \frac{6x_t y_t}{1 + 0.5x_t} \quad (6)$$

The bifurcation parameter l was linearly increased from 3.48 to 3.78 throughout the whole simulated time series. Following Dakos *et al.* (*41*), we used a stochastic modeling framework. We applied process noise on the state variable (x_t or N_t) based on Gaussian white noise, ωx_t. The noise was multiplied by ζ as ζx_t or ζN_t. As a consequence, the SD of the noise is ζ times of the value of the previous time step.

For each model, we generated the time series. First, we chose the fixed parameters (i.e., the parameters other than the tuning bifurcation parameter) by determining the equilibrium in the absence of noise with the bifurcation parameter at the initial value. Subsequently, we used the time series variables at equilibrium as the initial values for modeling the stochastic system. By doing so, we avoided the burn-in period. Last, we generated the time series while gradually changing the bifurcation parameter. For each simulation, we generated a time series of 10,000 points as in the study of Dakos *et al.* (*30*).

Empirical data

We applied the DEV approach (explained in the DEV analysis section below) on five empirical datasets: (i) cyanobacteria under light stress in a microcosm (*27*), (ii) phonation onset under increasing flow rate, (iii) cytosolic ATP dynamics in living plant tissues under progressing hypoxia (*52*), (iv) calcium carbonate ($CaCO_3$) concentrations in sediments before the end of last greenhouse Earth (*2*), and (v) bus voltage frequency before the North Western U.S. power grid failure in 1996 (*53*).

Cyanobacteria under light stress

We reanalyzed the response of a cyanobacteria population in chemostats to dilution events under a regime of gradually increasing light level (*27*, *54*). Population density was determined as the light attenuation coefficient calculated from continuous measurements of the outgoing light intensity. In total, this time series includes 7784 data points spanning overall 28.86 days with time interval equal to 0.0035 day (5 min) (*54*). It is noteworthy that the overall time series consists of six segments separated by dilution events (Fig. 3A and table S1). Since dilution events are not part of the population dynamics, we only analyzed time series segments after recovery from the previous dilution event and before undergoing the new dilution event. Because the shortest continuous segment (the one before dilution event P2) was 250 time points long (~1 day), to be consistent for all dilution events, we used only the last 250 data points before each dilution event when analyzing all the segments (P1 to P6; in total $6 \times 250 = 1500$ data points).

Phonation onset under increasing flow

Phonation onset (i.e., onset of vocal fold oscillation) is regarded as a Hopf bifurcation in the framework of dynamical systems (*55*). To experimentally realize the phonation onset using a physical replica of the vocal folds, the EPI (i.e. "epithelium") model was constructed following an established procedure (*56*). In accordance with the real vocal fold physiology, the EPI model had a body-cover structure. The cover layer was based on an extremely flexible superficial layer of the lamina propria (SLLP), covered by a thin epithelium layer. The SLLP layer was attached to the body layer with a support of ligament layer. The individual layers having different stiffness and strength were produced by silicone materials. With the detailed multilayer structure, the EPI model oscillates with a pronounced convergent-divergent motion, resembling the real vocal fold oscillations.

The experimental setup to realize flow-induced oscillations of the vocal fold model has been described (*57*). In this experiment, no supraglottal tube was attached. The subglottal pressure was measured by a pressure transducer (differential pressure transducer, PDS 70GA, Kyowa; signal conditioner, CDV 700A, Kyowa), located 2 cm upstream of the vocal fold model, and recorded with 44-kHz sampling rate. During the experiment of phonation onset, the flow rate was slowly increased until the vocal folds started to oscillate. From this experiment, we obtained time series data including 7501 data points, spanning an overall of 0.375 s with time interval equal to 5×10^{-5} s (Fig. 3D and table S1).

Cellular energy status under hypoxia

The data represent the dynamics of ATP concentration in the cytosol of living leaf cells over time and were measured by fluorimetry using an intracellular Förster resonance energy transfer (FRET) sensor that responds to $MgATP^{2-}$. In the dark, leaves respire and gradually deplete the ambient oxygen within a sealed compartment. This leads to an onset of cellular hypoxia and triggers a drop in energy charge. The ATP remained relatively stable while oxygen was gradually depleted and then suddenly dropped (Fig. 3G). This drop appeared to occur before the oxygen concentration became limiting for the mitochondrial respiratory chain, which is responsible for most cellular ATP production. How the stabilization

and the collapse of ATP are modulated mechanistically in the living cell remains to be resolved.

The data represented the fluorescent readout of a genetically encoded fluorescent protein-based FRET sensor that indicated ambient concentration of the biological energy carrier molecule ATP (i.e., its dominant bioavailable form in the cell, $MgATP^{2-}$) (*58*). The sensor (ATeam 1.03 nD/nA) consisted of a blue fluorescent protein [the cyan fluorescent protein (CFP) derivative mseCFP], a yellow fluorescent protein (YFP; the YFP derivative cp178-mVenus), and an ATP-binding domain (ε-subunit from *Bacillus subtilis* F_oF_1-ATP synthase) (*58*). The more $MgATP^{2-}$ is present in the direct environment of the protein, the higher the FRET, meaning that the fluorescence emission of the YFP acceptor increased, whereas that of the CFP donor simultaneously decreased. For the measurement, the sensor protein is genetically expressed in the cytosol of leaves of the model plant *Arabidopsis thaliana* (5- to 6-week-old plant) (*59*). Leaf slices (30-mg fresh weight) were placed in a single well of a 96-well multititer plate (*52*). The well was filled with medium and sealed with a transparent, air-tight film to prevent oxygen diffusion. In the dark, the tissue respires off the available oxygen in the medium, which turns gradually hypoxic. After sealing the well and initiating fluorescence recording, the sensor indicated a slight gradual decline of cytosolic $MgATP^{2-}$ up to a point, at which the FRET ratio suddenly decreased, indicating that cytosolic $MgATP^{2-}$ concentrations collapsed (Fig. 3D). The fluorescence of the leaf tissue was measured every 40 s, the background fluorescence was subtracted for isolating the sensor signal, and the fluorescence emission ratio YFP/CFP was calculated. Five biological replicates were measured with similar observations, and the experiment was repeated twice. The dataset analyzed here was reported recently (*52*). From this experiment, we obtained time series data including 271 data points, spanning an overall of 3 min with time interval equal to 0.011 min (Fig. 3G and table S1).

Calcium carbonate in the end of greenhouse Earth

We reanalyzed the calcium carbonate ($CaCO_3$) time series associated to the end of greenhouse Earth (*2*) that marked the transition of an ice cap–free Earth to an Earth with ice caps on the poles. In this study, the authors had reported that the time series had an increase in autocorrelation while approaching the climate shift. In total, this time series includes 462 data points, spanning an overall of 5.9 million years with time interval equal to 0.013 million years (Fig. 3J and table S1).

Bus voltage frequency before power grid failure

We analyzed bus voltage frequency data measured before the Western Interconnect Blackout of August 1996. The time series consisted of ~10 min of measurements at a sampling rate of $\Delta t = 0.05$ s from the Bonneville Power Administration territory, until the point of separation. A similar time series (with a $\Delta t = 0.02415$ s) have been shown to exhibit critical fluctuation approaching the point of blackout (*60*). For our study, data were prepared in the same way as in the previous study (*60*). In total, this time series included 11301 data points, spanning an overall of 565 s (Fig. 3M and table S1).

DEV analysis

The most critical step for the DEV approach is to reconstruct the attractor. As system dynamics may change through time, we used a windowing approach, instead of estimating the Jacobians using the whole time series at once, as was done by Ushio *et al.* (*18*). Thus, a proper window size, w (i.e., length of time series segment for estimating DEV), is needed to be chosen for each time series analysis to best describe the associated dynamics of the system. In addition, best embedding dimension, E, and time lag, τ, are needed to be estimated.

As in previous publications applying S-map (see detailed explanation in the "EWS based on the dominant eigenvalue" section), we screened for the parameter orchestration resulting in the best performance [i.e., S-map prediction skill (*61*)]. To determine the optimal window size for computation, we screened various window sizes. For each window size, we evaluated S-map skill (predictability, ρ) for various combinations of embedding dimensions E (1 to 12) and time lags τ (1 to 12) and obtained the highest ρ (ρ_{max}). During this stage of searching the optimal window size, for simplifying the calculation, we chose $\theta = 0$ in S-map, following the recommendation of Hsieh *et al.* (*61*). When $\theta = 0$, S-map is equivalent to an autoregressive model of order E (*61*). The optimal window size (w) close to the plateau was determined visually, beyond which increasing the window size leads to very minor improvement of the predictability (fig. S2A). Considering the paucity of time series data and avoiding the risk of overfitting, we chose the window size closest to the plateau phase. The best E and τ associated with the optimal window size resulting in best ρ were used throughout the analysis. Then, sensitivity analyses for various E, τ, and w should be done to ensure the robustness of results. Selected parameters for the SSR of each dataset are summarized in table S1.

After determining w, E, and τ, we proceeded to estimate the time series of Jacobian for the window segment (fig. S2, B to D). To account for changing nonlinearity of the reconstructed attractor (*41*), for each time series segment defined by the moving window, S-map analyses were run for various θ (0 to 2.5); the best θ giving the best S-map forecast skill was chosen. After obtaining the time series of Jacobian, we subsequently calculated the dominant eigenvalue at each time point within the window. Then, we averaged all eigenvalues derived in the time window as our DEV indicator. The averaging process smoothed out the uncertainty of estimating DEV at each time point; in addition, the averaged DEV indicated the vulnerability to critical transition for that region of attractor. Last, moving the window forward and repeating the calculation for every time step, we obtained the time series of DEV. The absolute value of DEV approaching 1 is indicative of critical transition. Using time series segments of the chosen window size, we consecutively estimated the EWSs. The signals were reported and matched to the time index associated with the last point of the window. For practical purposes, one can use a simple linear regression between DEV versus time to make an extrapolation (Fig. 3), to visualize and anticipate the occurrence of critical transition. It is also possible to fit a nonlinear curve, if the DEV approaches 1 nonlinearly.

Sensitivity of DEV approach to stochasticity

Noise (process and observation error) may undermine the efficacy of DEV. Thus, we examined effects of noise on the three mathematical models. To create observation error, after generating a time series, observation error was added by substituting each time point x_t by a normally distributed random value with mean x_t and SD ϕ, where ϕ determines the level of observation noise. The process error was intrinsically included in our stochastic models. To increase process noise, we increased the parameter ζ (see the "Model data" section).

For a given combination of process noise and observation error (see figs. S4 to S7 for the combinations), 100 simulations were run for each model. For each run, the DEV estimates at the first window and the window immediately before bifurcation were used for further analyses. By this procedure, we demonstrated (i) quantitative and (ii) qualitative properties of the DEV as an EWS: (i) Because mathematically the absolute value of the dominant eigenvalue is 1 at bifurcation, the estimated DEV should be close to 1, too, to be a robust quantitative indicator. (ii) Furthermore, the eigenvalues are expected to increase before bifurcation. Thus, ΔDEV, defined as the difference between DEV before bifurcation and the DEV at the initial phase of the simulation, was calculated to demonstrate that DEV was a qualitative EWS.

Note that for the Rosenzweig-MacArthur model, even intermediate level of process noise results in breakdown of the system (infinite values); thus, only limited level of process noise can be examined (fig. S6).

Comparison with AR1 and variance

For comparative purposes, all data were also analyzed using the two most commonly used resilience indicators, autocorrelation and variance. We estimated one-lag autocorrelation (AR1) as the Pearson correlation for lagged time series at one point, and variance as the SD. We used the same window size as that for the DEV approach to make results comparable. Before analysis, linear trends in the time series segment were removed using simple regression.

Computation

All analyses were done with R (version 3.1.2). The S-map analyses were implemented using rEDM. AR1 and variances were computed using the built-in functions in R. Documentation of all the analytical procedures and R codes mentioned above is provided in Zenodo repository, https://doi.org/10.5281/zenodo.7379358.

Supplementary Materials

This PDF file includes:

Supplementary Text
Figs. S1 to S17
Tables S1 and S2
References

View/request a protocol for this paper from *Bio-protocol*.

REFERENCES AND NOTES

1. M. Scheffer, S. Carpenter, J. A. Foley, C. Folke, B. Walker, Catastrophic shifts in ecosystems. *Nature* **413**, 591–596 (2001).
2. V. Dakos, M. Scheffer, E. H. van Nes, V. Brovkin, V. Petoukhov, H. Held, Slowing down as an early warning signal for abrupt climate change. *Proc. Natl. Acad. Sci. U.S.A.* **105**, 14308–14312 (2008).
3. M. Scheffer, S. R. Carpenter, T. M. Lenton, J. Bascompte, W. Brock, V. Dakos, J. van de Koppel, I. A. van de Leemput, S. A. Levin, E. H. van Nes, M. Pascual, J. Vandermeer, Anticipating critical transitions. *Science* **338**, 344–348 (2012).
4. C. M. Topaz, M. R. D'Orsogna, L. Edelstein-Keshet, A. J. Bernoff, Locust dynamics: Behavioral phase change and swarming. *PLOS Comp. Biol.* **8**, e1002642 (2012).
5. I. A. van de Leemput, M. Wichers, A. O. J. Cramer, D. Borsboom, F. Tuerlinckx, P. Kuppens, E. H. van Nes, W. Viechtbauer, E. J. Giltay, S. H. Aggen, C. Derom, N. Jacobs, K. S. Kendler, H. L. J. van der Maas, M. C. Neale, F. Peeters, E. Thiery, P. Zachar, M. Scheffer, Critical slowing down as early warning for the onset and termination of depression. *Proc. Natl. Acad. Sci. U.S.A.* **111**, 87–92 (2014).
6. P. U. Clark, N. G. Pisias, T. F. Stocker, A. J. Weaver, The role of the thermohaline circulation in abrupt climate change. *Nature* **415**, 863–869 (2002).
7. M. Scheffer, J. Bascompte, W. A. Brock, V. Brovkin, S. R. Carpenter, V. Dakos, H. Held, E. H. van Nes, M. Rietkerk, G. Sugihara, Early-warning signals for critical transitions. *Nature* **461**, 53–59 (2009).
8. H. Egbert, Slow recovery from perturbations as a generic indicator of a nearby catastrophic shift. *Am. Nat.* **169**, 738–747 (2007).
9. S. H. Strogatz, *Nonlinear Dynamics and Chaos: With Applications to Physics, Biology, Chemistry, and Engineering* (CRC Press, ed. 2, 2015), p. 531.
10. C. Wissel, A universal law of the characteristic return time near thresholds. *Oecologia* **65**, 101–107 (1984).
11. V. Dakos, E. H. van Nes, P. D'Odorico, M. Scheffer, Robustness of variance and autocorrelation as indicators of critical slowing down. *Ecology* **93**, 264–271 (2012).
12. S. Kéfi, V. Dakos, M. Scheffer, E. H. Van Nes, M. Rietkerk, Early warning signals also precede non-catastrophic transitions. *Oikos* **122**, 641–648 (2013).
13. V. Dakos, S. R. Carpenter, E. H. van Nes, M. Scheffer, Resilience indicators: Prospects and limitations for early warnings of regime shifts. *Philos. Trans. R. Soc. B Biol. Sci.* **370**, 20130263 (2015).
14. E. Weinans, R. Quax, E. H. van Nes, I. A. van de Leemput, Evaluating the performance of multivariate indicators of resilience loss. *Sci. Rep.* **11**, 9148 (2021).
15. T. M. Bury, R. I. Sujith, I. Pavithran, M. Scheffer, T. M. Lenton, M. Anand, C. T. Bauch, Deep learning for early warning signals of tipping points. *Proc. Natl. Acad. Sci. U.S.A.* **118**, e2106140118 (2021).
16. M. Scheffer, S. R. Carpenter, V. Dakos, E. H. van Nes, Generic indicators of ecological resilience: Inferring the chance of a critical transition. *Annu. Rev. Ecol. Evol. Syst.* **46**, 145–167 (2015).
17. Y. A. Kuznetsov, *Elements of Applied Bifurcation Theory* (Springer Science & Business Media, 2013), vol. 112.
18. M. Ushio, C. H. Hsieh, R. Masuda, E. R. Deyle, H. Ye, C. W. Chang, G. Sugihara, M. Kondoh, Fluctuating interaction network and time-varying stability of a natural fish community. *Nature* **554**, 360–363 (2018).
19. S. Cenci, S. Saavedra, Non-parametric estimation of the structural stability of non-equilibrium community dynamics. *Nat. Ecol. Evol.* **3**, 912–918 (2019).
20. H. Ye, R. J. Beamish, S. M. Glaser, S. C. Grant, C. H. Hsieh, L. J. Richards, J. T. Schnute, G. Sugihara, Equation-free mechanistic ecosystem forecasting using empirical dynamic modeling. *Proc. Natl. Acad. Sci. U.S.A.* **112**, E1569–E1576 (2015).
21. A. R. Ives, V. Dakos, Detecting dynamical changes in nonlinear time series using locally linear state-space models. *Ecosphere* **3**, art58 (2012).
22. F. Takens, in *Dynamic Systems and Turbulence*, D. A. Rand, L. S. Young, Eds. (Springer-Verlag, 1981), pp. 366–381.
23. M. Golubitsky, I. Stewart, D. G. Schaeffer, *Singularities and Groups in Bifurcation Theory: Volume II* (Springer Science & Business Media, 2012), vol. 69.
24. C.-W. Chang, T. Miki, M. Ushio, P. J. Ke, H. P. Lu, F. K. Shiah, C. H. Hsieh, Reconstructing large interaction networks from empirical time series data. *Ecol. Lett.* **24**, 2763–2774 (2021).
25. E. R. Deyle, R. M. May, S. B. Munch, G. Sugihara, Tracking and forecasting ecosystem interactions in real time. *Proc. R. Soc. Lond. B Biol. Sci.* **283**, 20152258 (2016).
26. W. C. Roda, M. B. Varughese, D. Han, M. Y. Li, Why is it difficult to accurately predict the COVID-19 epidemic? *Infect. Dis. Model.* **5**, 271–281 (2020).
27. A. J. Veraart, E. J. Faassen, V. Dakos, E. H. van Nes, M. Lürling, M. Scheffer, Recovery rates reflect distance to a tipping point in a living system. *Nature* **481**, 357–359 (2012).
28. N. Sun, R. J. Youle, T. Finkel, The mitochondrial basis of aging. *Mol. Cell* **61**, 654–666 (2016).
29. J. Nunnari, A. Suomalainen, Mitochondria: In sickness and in health. *Cell* **148**, 1145–1159 (2012).
30. V. Dakos, S. R. Carpenter, W. A. Brock, A. M. Ellison, V. Guttal, A. R. Ives, S. Kéfi, V. Livina, D. A. Seekell, E. H. van Nes, M. Scheffer, Methods for detecting early warnings of critical transitions in time series illustrated using simulated ecological data. *PLOS ONE* **7**, e41010 (2012).
31. A. Hastings, D. B. Wysham, Regime shifts in ecological systems can occur with no warning. *Ecol. Lett.* **13**, 464–472 (2010).
32. S. R. Carpenter, W. A. Brock, Early warnings of regime shifts in spatial dynamics using the discrete Fourier transform. *Ecosphere* **1**, art10 (2010).
33. V. Dakos, E. H. van Nes, R. Donangelo, H. Fort, M. Scheffer, Spatial correlation as leading indicator of catastrophic shifts. *Theor. Ecol.* **3**, 163–174 (2010).
34. S. Kéfi, V. Guttal, W. A. Brock, S. R. Carpenter, A. M. Ellison, V. N. Livina, D. A. Seekell, M. Scheffer, E. H. van Nes, V. Dakos, Early warning signals of ecological transitions: Methods for spatial patterns. *PLOS ONE* **9**, e92097 (2014).
35. S. Chen, E. B. O'Dea, J. M. Drake, B. I. Epureanu, Eigenvalues of the covariance matrix as early warning signals for critical transitions in ecological systems. *Sci. Rep.* **9**, 2572 (2019).

36. S. Tang, S. Allesina, Reactivity and stability of large ecosystems. *Front. Ecol. Evol.* **2**, 1–8 (2014).
37. T. Okada, A. Mochizuki, Law of localization in chemical reaction networks. *Phys. Rev. Lett.* **117**, 048101 (2016).
38. T. Okada, A. Mochizuki, M. Furuta, J.-C. Tsai, Flux-augmented bifurcation analysis in chemical reaction network systems. *Phys. Rev. E* **103**, 062212 (2021).
39. A. Aparicio, J. X. Velasco-Hernández, C. H. Moog, Y.-Y. Liu, M. T. Angulo, Structure-based identification of sensor species for anticipating critical transitions. *Proc. Natl. Acad. Sci. U.S.A.* **118**, e2104732118 (2021).
40. S. Cenci, G. Sugihara, S. Saavedra, Regularized S-map for inference and forecasting with noisy ecological time series. *Methods Ecol. Evol.* **10**, 650–660 (2019).
41. V. Dakos, S. M. Glaser, C. H. Hsieh, G. Sugihara, Elevated nonlinearity as an indicator of shifts in the dynamics of populations under stress. *J. R. Soc. Interface* **14**, 20160845 (2017).
42. W. D. Dechert, R. Gençay, The topological invariance of Lyapunov exponents in embedded dynamics. *Phys. D Nonlinear Phenom.* **90**, 40–55 (1996).
43. Y. A. Kuznetsov, *Elements of Applied Bifurcation Theory* (Springer, 2004), p. 634.
44. E. Deyle, G. Sugihara, Generalized theorems for nonlinear state space reconstruction. *PLOS ONE* **6**, e18295 (2011).
45. T. Sauer, J. A. Yorke, M. Casdagli, Embedology. *J. Stat. Phys.* **65**, 579–616 (1991).
46. H. Kantz, T. Schreiber, *Nonlinear Time Series Analysis* (Cambridge Univ. Press, ed. 2, 2010).
47. J. P. Eckmann, D. Ruelle, in *The Theory of Chaotic Attractors*, B. R. Hunt, T.-Y. Li, J. A. Kennedy, H. E. Nusse, Eds. (Springer New York, 2004), pp. 273–312.
48. M. Sano, Y. Sawada, Measurement of the Lyapunov spectrum from a chaotic time series. *Phys. Rev. Lett.* **55**, 1082–1085 (1985).
49. I. Noy-Meir, Stability of grazing systems: An application of predator-prey graphs. *J. Ecol.* **63**, 459–481 (1975).
50. M. Hénon, in *The Theory of Chaotic Attractors*, B. R. Hunt, T.-Y. Li, J. A. Kennedy, H. E. Nusse, Eds. (Springer New York, 1976), pp. 94–102.
51. M. L. Rosenzweig, R. H. MacArthur, Graphical representation and stability conditions of predator-prey interactions. *Am. Nat.* **97**, 209–223 (1963).
52. S. Wagner, J. Steinbeck, P. Fuchs, S. Lichtenauer, M. Elsässer, J. H. M. Schippers, T. Nietzel, C. Ruberti, O. van Aken, A. J. Meyer, J. T. van Dongen, R. R. Schmidt, M. Schwarzländer, Multiparametric real-time sensing of cytosolic physiology links hypoxia responses to mitochondrial electron transport. *New Phytol.* **224**, 1668–1684 (2019).
53. Western Systems Coordinating Council, "Western Systems Coordinating Council disturbance report for the power system outages that occurred on the Western Interconnection on July 2, 1996 and July 3, 1996" (Western Systems Coordinating Council, 1996).
54. A. J. Veraart, E. J. Faassen, V. Dakos, E. H. van Nes, M. Lürling, M. Scheffer, Recovery rates reflect distance to tipping point in a living system. *Nature* **481**, 357–359 (2011).
55. P. Mergell, H. Herzel, T. Wittenberg, M. Tigges, U. Eysholdt, Phonation onset: Vocal fold modeling and high-speed glottography. *J. Acoust. Soc. Am.* **104**, 464–470 (1998).
56. P. R. Murray, S. L. Thomson, Vibratory responses of synthetic, self-oscillating vocal fold models. *J. Acoust. Soc. Am.* **132**, 3428–3438 (2012).
57. R. Shimamura, I. T. Tokuda, Effect of level difference between left and right vocal folds on phonation: Physical experiment and theoretical study. *J. Acoust. Soc. Am.* **140**, 3393–3394 (2016).
58. H. Imamura, K. P. Huynh Nhat, H. Togawa, K. Saito, R. Iino, Y. Kato-Yamada, T. Nagai, H. Noji, Visualization of ATP levels inside single living cells with fluorescence resonance energy transfer-based genetically encoded indicators. *Proc. Natl. Acad. Sci. U.S.A.* **106**, 15651–15656 (2009).
59. V. De Col, P. Fuchs, T. Nietzel, M. Elsässer, C. P. Voon, A. Candeo, I. Seeliger, M. D. Fricker, C. Grefen, I. M. Møller, A. Bassi, B. L. Lim, M. Zancani, A. J. Meyer, A. Costa, S. Wagner, M. Schwarzländer, ATP sensing in living plant cells reveals tissue gradients and stress dynamics of energy physiology. *eLife* **6**, e26770 (2017).
60. E. Cotilla-Sanchez, P. D. H. Hines, C. M. Danforth, Predicting critical transitions from time series synchrophasor data. *IEEE Trans. Smart Grid* **3**, 1832–1840 (2012).
61. C.-h. Hsieh, S. M. Glaser, A. J. Lucas, G. Sugihara, Distinguishing random environmental fluctuations from ecological catastrophes for the North Pacific Ocean. *Nature* **435**, 336–340 (2005).
62. R. M. May, Simple mathematical models with very complicated dynamics. *Nature* **261**, 459–467 (1976).
63. P. S. Dutta, Y. Sharma, K. C. Abbott, Robustness of early warning signals for catastrophic and non-catastrophic transitions. *Oikos* **127**, 1251–1263 (2018).
64. A. A. Arkilanian, C. F. Clements, A. Ozgul, G. Baruah, Effect of time series length and resolution on abundance- and trait-based early warning signals of population declines. *Ecology* **101**, e03040 (2020).

Acknowledgments: We thank S. Wagner (Cologne, Germany) for the original recording of the published data on cellular energy status at hypoxia analyzed in this work. We thank the Bonneville Power Administration for providing the frequency dataset. We are grateful for comments from G. Sugihara, L.-Y. Chiao, and J.-C. Tsai and English editing by J. Kastelic that improved our work. **Funding:** This work was supported by the National Center for Theoretical Sciences, National Taiwan University, Academia Sinica, Foundation for the Advancement of Outstanding Scholarship, and the National Science and Technology Council, Taiwan (to C.-h.H. and C.-W.C.). **Author contributions:** C.-h.H., F.G., and A.T. conceived the research idea; F.G. and C.-W.C. developed the methods and analyzed the models and data, with help from V.D., C.-h.H., A.T., and E.H.v.N.; V.D., M.H., O.K., M.S., and I.T.T. provided data; C.-W.C., C.-h.H., F.G., and A.T. wrote the manuscript with comments from all co-authors. **Competing interests:** The authors declare that they have no competing interests. **Data and materials availability:** All data needed to evaluate the conclusions in the paper are present in the paper and/or the Supplementary Materials. Dataset and the documentation of all analytical procedures provided as R codes are available in online Zenodo repository, https://doi.org/10.5281/zenodo.7379358.

Submitted 9 April 2022
Accepted 2 December 2022
Published 6 January 2023
10.1126/sciadv.abq4558

ScienceAdvances

Anticipating the occurrence and type of critical transitions

Florian Grziwotz, Chun-Wei Chang, Vasilis Dakos, Egbert H. van Nes, Markus Schwarzlnder, Oliver Kamps, Martin Heler, Isao T. Tokuda, Arndt Telschow, and Chih-hao Hsieh

Sci. Adv., **9** (1), eabq4558.
DOI: 10.1126/sciadv.abq4558

Science Advances (ISSN) is published by the American Association for the Advancement of Science. 1200 New York Avenue NW, Washington, DC 20005. The title *Science Advances* is a registered trademark of AAAS.